



## Original

# Comparison of the anatomical morphology of cervical vertebrae between humans and macaques: related to a spinal cord injury model

Junhao LIU, Zhou YANG, Xiuhua WU, Zucheng HUANG, Zhiping HUANG, Xushi CHEN, Qi LIU, Hui JIANG and Qingan ZHU

Division of Spinal Surgery, Department of Orthopaedics, Nanfang Hospital, Southern Medical University, 1838 North Guangzhou Avenue, Guangzhou, China

**Abstract:** Non-human primates are most suitable for generating cervical experimental models, and it is necessary to study the anatomy of the cervical spine in non-human primates when generating the models. The purpose of this study was to provide the anatomical parameters of the cervical spine and spinal cord in long-tailed macaques (*Macaca fascicularis*) as a basis for cervical spine-related experimental studies. Cervical spine specimens from 8 male adult subjects were scanned by micro-computed tomography, and an additional 10 live male subjects were scanned by magnetic resonance imaging. The measurements and parameters from them were compared to those of 12 male adult human subjects. Additionally, 10 live male subjects were scanned by magnetic resonance imaging, and the width and depth of the spinal cord and spinal canal and the thickness of the anterior and posterior cerebrospinal fluid were measured and compared to the relevant parameters of 10 male adult human subjects. The tendency of cervical parameters to change with segmental changes was similar between species. The vertebral body, spinal canal, and spinal cord were significantly flatter in the human subjects than in the long-tailed macaques. The cerebrospinal fluid space in the long-tailed macaques was smaller than that in the human subjects. The anatomical features of the cervical vertebrae of long-tailed macaques provide a reference for establishing a preclinical model of cervical spinal cord injury.

**Key words:** anatomical parameters, cervical spine, non-human primate, spinal cord injury model

## Introduction

Rodent are the most widely used animal in experimental research [1–4], though some research involves the use of calves, deer, and pigs, which are considered large animal models [5–7]. However, some differences may exist in the spine structure that could limit the application of the aforementioned animals as biomechanical models or spinal cord injury models. For example, the growth direction of the spine in the aforementioned animals is not consistent with that in human subjects, indicating that the biomechanical structures might be different between tetrapods and human subjects. In addition, differ-

ences in neuroanatomical functions and repair mechanisms after nerve injury further limit their applications. It is well known that non-human primates are phylogenetically close to human subjects, so the results obtained from them are more instructive for preclinical studies than those in other experimental animals.

At present, non-human primates are increasingly being used in such fields as: viral hepatitis [8]; HIV/AIDS [9]; nervous system diseases, such as Alzheimer's disease (AD) [10]; spinal cord injury (SCI) [11, 12]; disorders related to social and psychological processes, such as anxiety [13] and depression [14]; cardiovascular diseases [15]; metabolic diseases, such as obesity [16] and

(Received 24 February 2020 / Accepted 14 September 2020 / Published online in J-STAGE 16 October 2020)

Corresponding author: Q. Zhu. e-mail: qinganzhu@gmail.com



This is an open-access article distributed under the terms of the Creative Commons Attribution Non-Commercial No Derivatives (by-nc-nd) License <<http://creativecommons.org/licenses/by-nc-nd/4.0/>>.

©2021 Japanese Association for Laboratory Animal Science

metabolic syndrome [17]; and respiratory diseases [18]. Therefore, it is necessary to understand the similarities and differences in functional and anatomical characteristics between non-human primates and human subjects. Furthermore, SCI often leads to permanent dysfunction, and the SCI model is of great significance for the study of this disease.

Previous studies had been conducted to measure parameters of the spine in mammals, and the anatomy of the baboon has been directly used to compare with the related structures in human subjects [19]. Some comparative anatomical analyses of cervical vertebrae between human subjects and non-human primates have also been conducted [20–24]. For example, Manfreda *et al.* [24] used geometric morphometry to study the relationship between the morphology of the atlas and the movement pattern of primates and indicated that the human atlas morphology may be a unique adaptation. Nalley *et al.* [21] assessed the morphology of the upper cervical vertebrae of primates and identified a significant association between the head and neck posture and the morphology of the cervical spine. Meyer *et al.* [23] evaluated the uncinate processes of existing primates to construct a cervical kinematics model of early fossil hominins. Nakatsukasa *et al.* [22] demonstrated that the bipedal movement of macaques after training is inconsistent with that of human subjects, which may be the result of a genetic limitation. For the nervous system, Thomas *et al.* [20] measured the distances between nerve root attachment points in rhesus macaques, long-tailed macaques, and baboons, including anterior and posterior distances and the distance between segments, and indicated that the difference in individual segment volumes between rhesus and long-tailed macaques (*Macaca mulatta* and *M. fascicularis*) was small but that the difference between the baboon and the other two species was large. These studies focused on the functional morphology of the cervical spine in terms of evolutionary biology. However, the anatomy of the cervical spine and spinal cord related to the SCI model in non-human primates remains unclear.

Some anatomical parameters, like disc height and axial area, have been used to estimate the anatomical performance of detached spinal segments [4, 25]. This research showed that these parameters can be applied to assess the anatomy of the cervical spine of non-human primates, such as long-tailed macaques, rhesus macaques, and baboons, and compare them to related structural parameters in human subjects.

The objective of this study was to provide a basis for establishing a preclinical experimental model related to cervical experiments by comparing the relevant morphol-

ogy of human subjects and long-tailed macaques (*Macaca fascicularis*) in various segments of the vertebrae and spinal cord. In the present study, we analyzed the anatomical features of the cervical spine and cervical spinal cord of the two species by measuring the relevant parameters of cervical vertebrae and spinal cord in computed tomography (CT; cadaver specimens) and magnetic resonance imaging (MRI; live subjects), respectively.

## Materials and Methods

### Animals and human subjects

Eight cervical long-tailed macaque cadaver and 10 live subjects of long-tailed macaques with a mean age of 8.2 years supplied by Landau Biotechnology Co., Ltd., were used in the present study. All procedures were conducted in accordance with the Guide for the Care and Use of Laboratory Animals (Institute of Laboratory Animal Resources, National Research Council, USA, 2011) and approved by the Institutional Animal Care And Use Committee (IACUC) of Guangdong Landau Biotechnology Co., Ltd., (Resolution No. LD-ZA-2016-01). The human subjects in the present study comprised a total of 22 normal males (12 for CT measurement and 10 for MRI measurement) with an average age of  $29.1 \pm 4.2$  years. The Ethics Committee of Nanfang Hospital, Southern Medical University, reviewed and approved the study, and the need for written consent from the participants was waived due to the retrospective design of the study.

### CT and MRI scans

The C2 to C7 vertebrae were harvested from each long-tailed macaque cadaver. High-resolution images were acquired using a Micro-CT scanner ( $\mu$ CT 80, Scanco Medical, Brüttisellen, Switzerland). A slice increment of 20  $\mu$ m and a 20.5 cm axial field of view were used to acquire the DICOM images of cadaver specimens. The live subjects were scanned in the prone position in a 3T MRI scanner (Verio, Siemens AG, Munich, Germany) to obtain sagittal and axial T1-weighted and T2-weighted sequences. Before scanning, the animals were first anesthetized by intramuscular injection of ketamine (5–10 mg/kg) and then anesthetized by intravenous injection of sodium pentobarbital (6–8 mg/kg). In addition, atropine (0.05 mg/kg) was used to inhibit saliva and bronchial secretion in animals. DICOM images were obtained with a 210  $\times$  210 mm axial field of view.

Scanning was performed on 22 normal male subjects with an average age of  $30.7 \pm 4.4$  years in Nanfang Hos-

pital. CT measurements were obtained from 12 subjects ( $28.5 \pm 3.4$  years), while the MRI measurements were obtained from 10 subjects ( $33.3 \pm 4.2$  years). The CT scans were performed with a CT scanner (Philips Brilliance 16 CT, Philips Medical Systems, Eindhoven, Netherlands) with a slice thickness of 1 mm, pitch of 0.7 mm, 120 kV, 180 mA, and  $512 \times 512$  matrix. The MR images were obtained with a 3T MRI scanner (GE Signa Excite) with a slice thickness of 4 mm, repetition time (TR)/echo time (TE) of 2,400/121 ms, field of view of  $240 \times 240$  mm, and  $512 \times 512$  matrix.

### Parameter collection and calculation

One observer used the RadiAnt DICOM VIEWER (Medixant, Poznań, Poland) and the other used OsiriX Lite 9.0 (Pixmeo SARL, Bernex, Switzerland) to make the measurements of macaques and human subjects, respectively. In addition, images of 3D-reconstruction of the whole cervical spine and each cervical vertebra were generated separately. The methods of measurements in our study refers to the previous studies [4, 19, 26]. The anteroposterior and lateral dimensions of the vertebrae, such as the depth and width of the vertebra (Vd and Vw, respectively), vertebral body (VBd and VBw, respectively), and spinal canal (SCd and SCw, respectively) were measured in axial views of CT scans. The heights of the vertebral body (VBh) and intervertebral disc (IVDh) were estimated in anterior views of CT scans as well (Figs. 1A and B, Table 1). The spinal cord (depth, SCod; width, SCow), spinal canal (depth, SCdM; width, SCwM), and cerebrospinal fluid (CSF, anterior depth, ACFd; posterior depth, PCFd) were measured in cross-sectional views of MRI scans (Figs 1C and D, Table 1). The same measurements were made 3 times by two independent operators and analyzed using the *t*-test, and there were no significant differences in any measurements between the two operators. Each linear parameter at each vertebral or spinal level in cadaver specimens and live subjects were computed as the average of the measurements. The averages at each spinal level were then also computed by using each parameter for each species. The axial morphology of the spine is reflected by the following three ratios: the vertebral width-to-depth (Vw/Vd), vertebral body width-to-depth (VBw/VBd), and spinal canal width-to-depth (SCw/SCd) ratio. The lateral morphology of the spine is reflected by the vertebral body height-to-depth (VBh/VBd). Moreover, the spinal cord parameters were measured by MRI, and the morphology of the spinal cord is represented by spinal cord width-to-depth (SCow/SCod) ratio. The data for all cases diagnosed as normal were included in the analyses. It is worth noting that the CT and MRI data

from the animal and human subjects in the present study did not come from the same individuals.

### Statistical analysis

SPSS Statistics 20.0 software was used to perform the statistical analysis in this study. A *t*-test was used for the comparison of the parameters between the two observers. For each species, the changes in every parameter across segments were analyzed using one-way ANOVA, and a post hoc Bonferroni test was used when there were significant differences in a one-way ANOVA. The Mann-Whitney test and Kruskal-Wallis test were used to compare the ratios between species and among segments, respectively, and a post hoc Dunn's test was used for multiple comparisons. A *P*-value of 0.05 was considered statistically significant.

## Results

### Comparison of the ratios between species

In general, most of the CT measurements were different between species. There were significant differences in Vw/Vd between species at C6 ( $P < 0.0011$ ) and C7 ( $P < 0.0001$ ). VBw/VBd at C5–7 and SCw/SCd at all segments were significantly different between species (Figs. 2A and B). There was only a significant difference in VBh/VBd between species at C3 (Fig. 2C). The IVDh/VBh ratio of the macaques was significantly greater than that of the human subjects (Fig. 2D). The VBw/Vw ratio of human subjects was greater than that of the macaques at C3–C7, whereas VBd/VD was significantly different between the species, except at C6 and C7 (Figs. 3A and B). In addition, there were no significant differences in SCw/Vw between species (Fig. 3C), and the SCd/VD ratio of the macaques was significantly greater than that of the human subjects (Fig. 3D).

Regarding the measurements of the spinal cord obtained with MRI images (Fig. 4), the SCow/SCod ratio of the human subjects was significantly greater than that of the macaques at each cervical segment (Fig. 4A). The SCow/SCwM and SCod/SCdM ratios of the human subjects were significantly smaller than those of macaques at C3–C7 (Figs. 4B and C). The ratio of the cerebrospinal fluid depth to the spinal cord depth (CFd/SCod) of the human subjects was significantly greater than that of the macaques at C3–C7 (Fig. 4D).

### Comparison of the measurements among segments in the human subjects

Regarding the cervical spine of the human subjects (Table 2), VBw was significantly greater at C6 and C7 than at C3 and C4, respectively, while VBh was signifi-

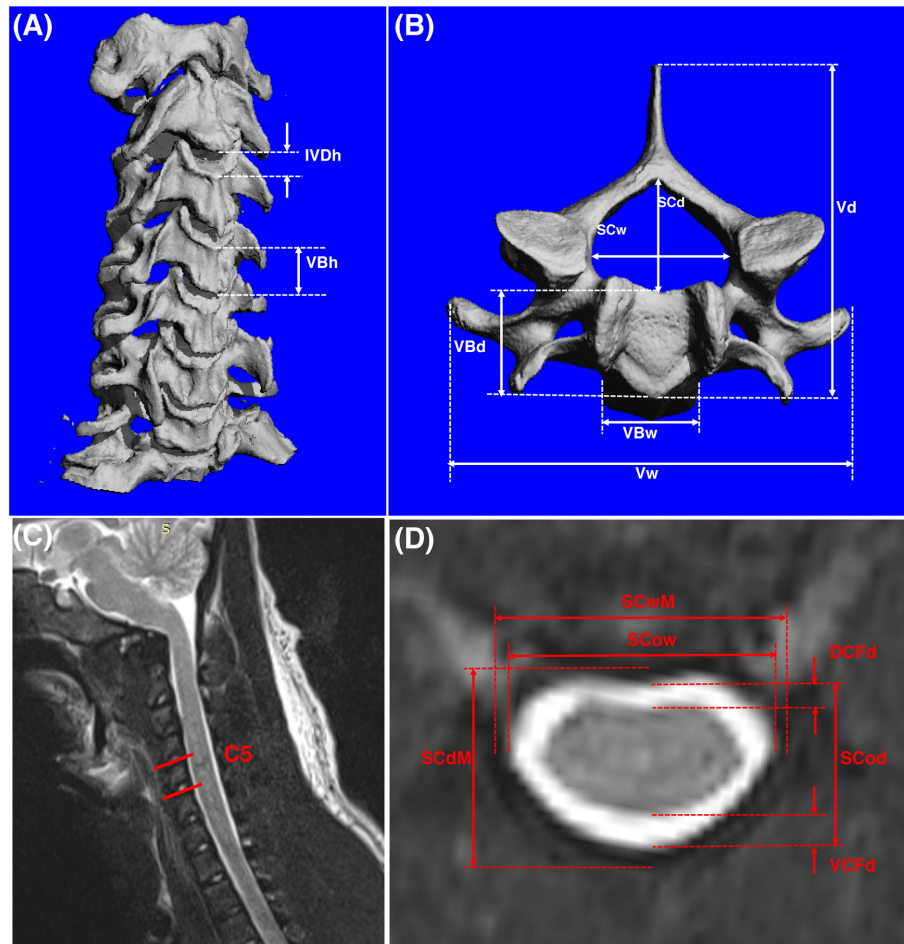


**Fig. 1.** Three-dimensional renderings of cervical vertebrae of an adult male long-tailed macaque, *Macaca fascicularis* (A and B). Cervical spinal cord of an adult male macaque (not to scale to show features) (C and D). The measured dimensions are indicated on the axial view of a cervical (C5) vertebra and on the right anterolateral view of the cervical spine. Vw, vertebral length; Vd, vertebral depth; VBw, vertebral body width; VBd, vertebral body depth; SCw, spinal canal width; SCd, spinal canal depth; VBh, vertebral body height; IVDh, intervertebral disc height. The measured dimensions are indicated on the axial view of a spinal cord (C5). SCow, spinal cord width; SCod, spinal cord depth; ACFd, anterior cerebrospinal fluid depth; PCFd, posterior cerebrospinal fluid depth; SCwM, spinal canal width scanned by MRI; SCdM, spinal canal depth scanned by MRI.

**Table 1.** The abbreviations to describe anatomical parameters

Abbreviation	Description
VBw	Maximum length of the vertebral body along the lateromedial direction, including the uncinat process.
VBd	Maximum vertebral length along the anteroposterior direction.
VBh	Measuring the length of the vertebral body from the superior aspect of its upper endplate to the inferior aspect of its lower endplate at the anterior edge of each vertebra.
Vw	Maximum length of the vertebra along the lateromedial direction.
Vd	Maximum length of the vertebra from anterior edge of vertebral body to spinous process along the anteroposterior direction.
SCw	Maximum lateral dimension of the spinal canal perpendicular to the midline.
SCd	Maximum length of the spinal canal along the anteroposterior direction.
IVDh	Length between the lower endplate of the superior vertebral body and the upper endplate of the lower vertebral body measured at the anterior edge of the vertebral body.
SCow	Maximum length of the spinal cord along the lateromedial direction.
SCod	Maximum length of the spinal cord along the anteroposterior direction
CFd	The distance between the dura and the spinal cord parenchyma on its corresponding side
ACFd	Maximum length between the anterior dura and the anterior spinal cord parenchyma
PCFd	Maximum length between the posterior dura and the posterior spinal cord parenchyma
SCwM	Maximum lateral dimension of the spinal canal perpendicular to the midline scanned by MRI
SCdM	Maximum length of the spinal canal along the anteroposterior direction scanned by MRI

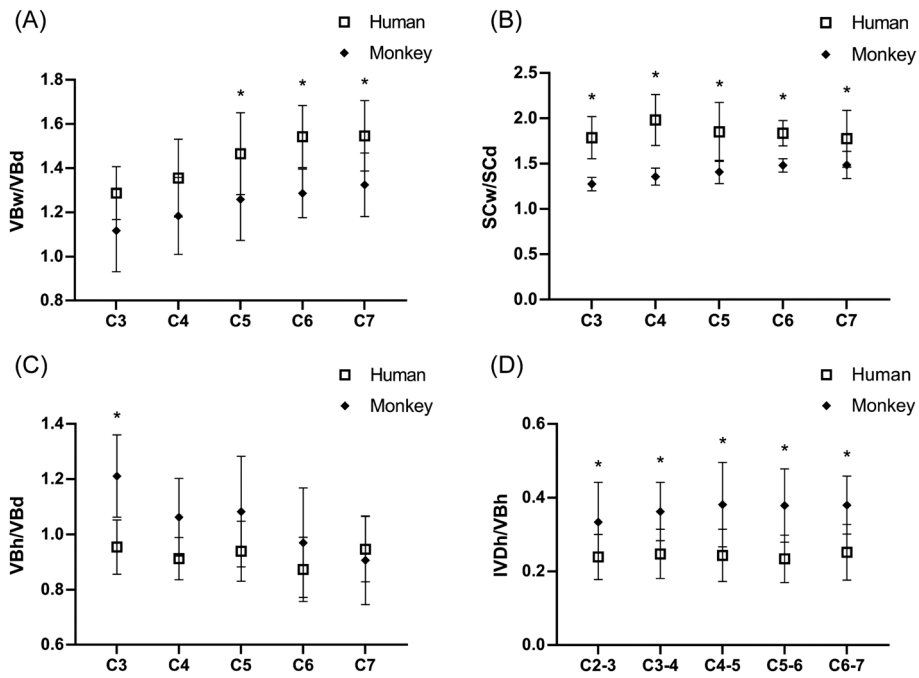


**Fig. 2.** Comparison of the anatomical ratios of the cervical spine between the human subjects and macaques. Significant differences ( $P < 0.05$ ) in corresponding segments between the human subjects and macaques are indicated with an asterisk (\*). (A)  $VBw/VBd$ , (B)  $SCw/SCd$ , (C)  $VBh/VBd$ , and (D)  $IVDh/VBh$ .  $VBw/VBd$ , vertebral body width-to-depth ratio;  $SCw/SCd$ , spinal canal width-to-depth ratio;  $VBh/VBd$ , vertebral body height-to-depth ratio;  $IVDh/VBh$ , intervertebral disc height to vertebral body height ratio. Variance bars represent the SD. The Mann-Whitney test was used to compare the ratios between species in corresponding segments.

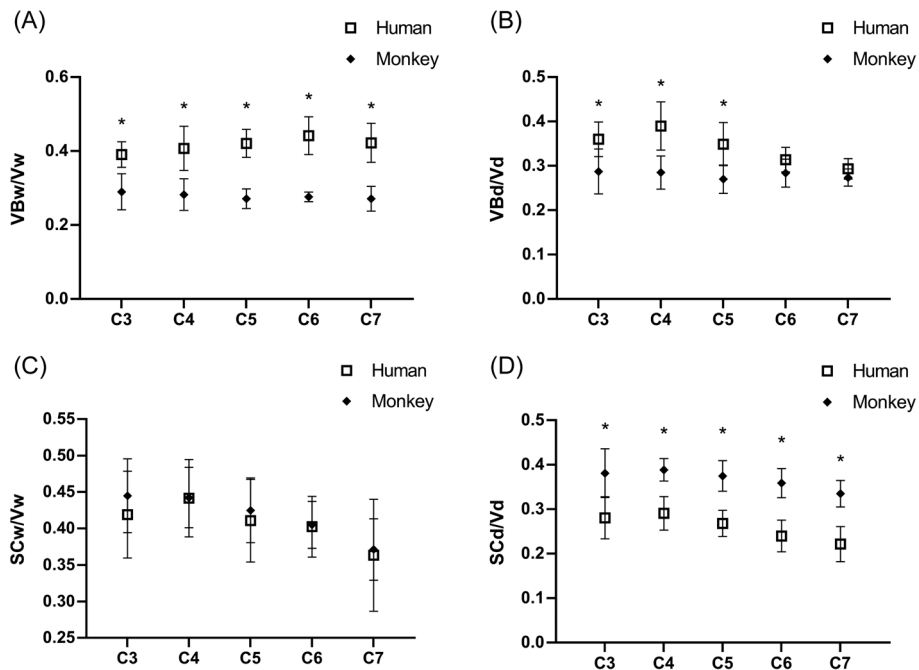


**Fig. 3.** Comparison of the anatomical ratio of the cervical spine between the human subjects and macaques. Significant differences ( $P < 0.05$ ) in corresponding levels between the human subjects and macaques are indicated with an asterisk (\*). (A)  $VBw/Vw$ , (B)  $VBd/Vd$ , (C)  $SCw/Vw$ , (D)  $SCd/Vd$ .  $VBw/Vw$ , vertebral body width to vertebral depth ratio;  $VBd/Vd$ , indicates vertebral body depth to vertebral depth ratio;  $SCw/Vw$ , spinal canal width to vertebral width ratio;  $SCd/Vd$ , spinal canal depth to vertebral depth ratio. Variance bars represent the SD. The Mann-Whitney test was used to compare the ratios between species in corresponding segments.

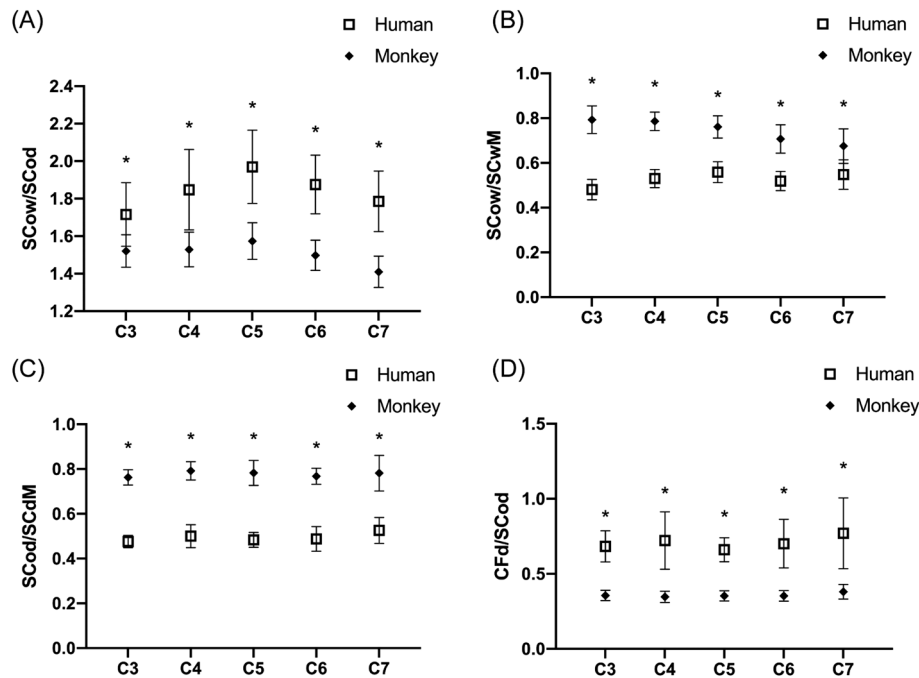


**Fig. 4.** Comparison of the anatomical ratio of the cervical spine between the human subjects and macaques as measured by MRI. Significant differences ( $P < 0.05$ ) in corresponding levels between the human subjects and macaques are indicated with an asterisk (\*). (A) SCow/SCod, (B) SCow/SCwM, (C) SCod/SCdM, and (D) CFd/SCod. SCow/SCod, spinal cord width-to-depth ratio; SCow/SCwM, spinal cord width to spinal canal width scanned by MRI ratio; SCod/SCdM, spinal cord depth to spinal canal depth scanned by MRI ratio; CFd/SCod, cerebrospinal fluid depth to spinal cord depth ratio. Variance bars represent the SD. The Mann-Whitney test was used to compare the ratios between species in corresponding segments.

cantly greater at C7 than that at C6. Vw and Vd were significantly greater at C7 than that at C3, C4, and C5, respectively, and Vd was also greater at C6 than at C3, C4, and C5. There were significant differences in Vw/Vd between C6, C7, and C4, respectively. The VBw/VBd ratio, which decreased cranially, was significantly greater at C6 and C7 than at C3, respectively (Table 2). The VBd/Vd ratio was smaller at C7 than at C3, C4, and C5, while there was no significant difference in VBw/Vw among segments. SCd/Vd was significantly smaller at C7 than at C3 and C4, respectively. There were no significant differences in the VBh/VBd, SCw/SCd, SCw/Vw, or IVDh/VBh ratios among segments (Table 2).

There were no significant differences in SCow, SCod, ACFd, PCFd, SCwM, or SCdM among segments (Table 3). The SCow/SCwM ratio was significantly greater at C5 than at C3, and there were no significant differences in SCow/SCod, SCod/SCdM, or CFd/SCod among segments (Table 3).

#### Comparison of the measurements among segments in macaques

Vw increased from C3 ( $23.35 \pm 3.92$  mm) to C7 ( $32.74 \pm 4.11$  mm), and Vw at C7 was significantly different from those at C3, C4, and C5 (Table 4). Also, SCw at

C6 and C7 was significantly greater at C6 and C7 than at C3. There were no significant differences in Vw/Vd, VBd/Vd, VBw/Vw, VBw/VBd, or IVDh/VBh. The SCw/SCd ratio was significantly greater at C6 and C7 than at C3, respectively. The VBh/VBd ratio was significantly lower at C7 than at C3. The SCw/Vw ratio was significantly smaller at C7 than at C3 and C4, and the SCd/Vd ratio was significantly smaller at C7 than at C4.

The posterior cerebrospinal fluid depth (PCFd) was significantly greater at C7 than at C5 and C6 (Table 5). Furthermore, SCwM was significantly larger at C6 and C7 than at C3 and C4 (Table 5). The SCow/SCod ratio was significantly smaller at C7 than at C5, and the SCow/SCwM ratio was significantly smaller at C6 and C7 than at C3 and C4, respectively. There were no significant differences in the SCod/SCdM or CFd/SCod ratios among segments (Table 5).

## Discussion

Anatomical comparisons between animals and human subjects have been reported in numerous studies [5, 6, 19, 26–28]. However, few studies have focused on the morphology of the cervical spine between human subjects and macaques, particularly to establish a preclinical

**Table 2.** Cervical anatomical measurements and ratios obtained by CT in human

	C3/C2-3	C4/C3-4	C5/C4-5	C6/C5-6	C7/C6-7
VBw (mm)	20.87 ± 2.01	22.18 ± 2.65	23.33 ± 2.13	26.01 ± 2.96†‡	27.13 ± 4.81†‡*
Vw (mm)	53.51 ± 3.13	54.69 ± 3.97	55.58 ± 3.69	59.07 ± 3.96	64.32 ± 9.34†‡*
VBd (mm)	16.30 ± 1.75	16.49 ± 1.70	16.11 ± 2.28	16.95 ± 2.05	17.56 ± 2.72
Vd (mm)	45.40 ± 3.77	42.62 ± 4.55	46.25 ± 3.57	54.40 ± 7.31†‡*	60.11 ± 8.86†‡*
SCw (mm)	22.43 ± 2.61	24.07 ± 2.47	22.80 ± 3.32	23.76 ± 2.33	22.87 ± 3.13
SCd (mm)	12.67 ± 1.60	12.31 ± 1.69	12.44 ± 1.45	13.00 ± 1.56	13.16 ± 2.04
VBh (mm)	15.45 ± 1.32	14.93 ± 1.03	14.96 ± 1.16	14.62 ± 1.02	16.41 ± 1.77#
IVDh (mm)	3.65 ± 0.86	3.70 ± 1.01	3.64 ± 1.12	3.40 ± 0.90	4.14 ± 1.20
Vw/Vd	1.18 ± 0.10	1.30 ± 0.16	1.21 ± 0.10	1.10 ± 0.12‡	1.07 ± 0.09‡
VBd/Vd	0.36 ± 0.04	0.39 ± 0.06	0.35 ± 0.05	0.31 ± 0.03‡	0.29 ± 0.02‡*
VBw/Vw	0.39 ± 0.03	0.41 ± 0.06	0.42 ± 0.04	0.44 ± 0.05	0.42 ± 0.05
VBw/VBd	1.29 ± 0.12	1.35 ± 0.18	1.47 ± 0.19	1.54 ± 0.14†	1.55 ± 0.16†
VBh/VBd	0.95 ± 0.10	0.91 ± 0.08	0.94 ± 0.11	0.87 ± 0.12	0.95 ± 0.12
SCw/SCd	1.79 ± 0.23	1.98 ± 0.28	1.85 ± 0.32	1.85 ± 0.14	1.77 ± 0.32
SCw/Vw	0.42 ± 0.06	0.44 ± 0.05	0.41 ± 0.06	0.40 ± 0.04	0.36 ± 0.08
SCd/Vd	0.28 ± 0.05	0.29 ± 0.04	0.27 ± 0.03	0.24 ± 0.03‡	0.22 ± 0.04‡†
IVDh/VBh	0.24 ± 0.06	0.25 ± 0.07	0.24 ± 0.07	0.23 ± 0.06	0.25 ± 0.07

Mean ± SD. Significant differences among vertebral segments in human are showed as C3 (†), and C4 (‡), C5 (\*), and C6 (#) ( $P < 0.05$ ). Shaded cells demonstrate a significant difference between the monkey and the human ( $P < 0.05$ ). A one-way ANOVA was used to compare the parameters among segments, and a post hoc Bonferroni test was used when there were significant differences on a one-way ANOVA. Kruskal-Wallis test was used to compare the ratios among segments, and a post hoc Dunn's test was used for multiple comparisons.

**Table 3.** Cervical anatomical measurements and ratios obtained by MRI in human

	C3	C4	C5	C6	C7
SCow (mm)	11.32 ± 0.91	12.22 ± 1.15	12.59 ± 0.70	12.28 ± 0.91	12.45 ± 1.50
SCod (mm)	6.62 ± 0.52	6.64 ± 0.48	6.43 ± 0.59	6.46 ± 0.38	6.98 ± 0.70
ACFd (mm)	2.40 ± 0.53	2.71 ± 1.10	2.07 ± 0.28	2.16 ± 0.62	3.19 ± 1.71
PCFd (mm)	2.10 ± 0.26	2.02 ± 0.38	2.16 ± 0.26	2.31 ± 0.50	2.27 ± 0.58
SCwM (mm)	23.55 ± 1.74	23.13 ± 1.73	22.62 ± 1.81	23.38 ± 2.11	22.75 ± 1.02
SCdM (mm)	13.99 ± 1.29	13.35 ± 1.78	13.30 ± 1.22	13.32 ± 1.12	13.30 ± 0.87
SCow/SCod	1.71 ± 0.17	1.84 ± 0.21	1.97 ± 0.20	1.87 ± 0.16	1.79 ± 0.16
SCow/SCwM	0.48 ± 0.05	0.53 ± 0.04	0.56 ± 0.05†	0.52 ± 0.04	0.55 ± 0.07
SCod/SCdM	0.48 ± 0.03	0.50 ± 0.05	0.48 ± 0.03	0.49 ± 0.05	0.53 ± 0.06
CFd/SCod	0.68 ± 0.10	0.72 ± 0.19	0.66 ± 0.08	0.70 ± 0.16	0.77 ± 0.24

Mean ± SD. Significant differences among vertebral segments in human are showed as C3 (†) ( $P < 0.05$ ). Shaded cells demonstrate a significant difference between the monkey and the human ( $P < 0.05$ ). A one-way ANOVA was used to compare the parameters among segments, and a post hoc Bonferroni test was used when there were significant differences on a one-way ANOVA. Kruskal-Wallis test was used to compare the ratios among segments, and a post hoc Dunn's test was used for multiple comparisons. Note: CFd=ACFd+PCFd.

model of SCI. The present study showed that the vertebral body, spinal canal, and spinal cord in the human subjects was flatter (greater width and smaller depth) than that in *the long-tailed macaques*. Additionally, the change in size and morphology of cervical vertebrae from the rostral to caudal side in the macaques was consistent with that in the human subjects. The cerebrospinal fluid (CSF) space, an important parameter for a spinal cord injury model, was found to be significantly different between the two species: the CSF space accounted for approximately 70% of the spinal canal in the human subjects and approximately 40% in the macaques ((ACSF+PCSF)/SCdM). These results provide a reference for establishing an SCI model using *the long-tailed macaques*.

The axial morphology of the C5, C6 and C7 vertebral bodies (VBw/VBd) was flatter in the human subjects than that in the macaques, while the sagittal view of the corresponding vertebral bodies revealed similar sagittal morphology between the human subjects and macaques. This may be due to differences in musculature and head-neck movement needs between human subjects and macaques [29]. In addition, the slenderness of the cervical spine was significantly greater in the macaques than in the human subjects (VBh/VBd and IVDh/VBd), and this indicates that macaques have a greater cervical range of mobility than human subjects [30]. The dynamic range of motion and neck slenderness may indicate that the spine of the macaques is more likely to be damaged [31], and the vertebral bodies, which were narrower in the

**Table 4.** Cervical anatomical measurements and ratios obtained by  $\mu$ CT in monkey

	C3/C2-3	C4/C3-4	C5/C4-5	C6/C5-6	C7/C6-7
VBw (mm)	6.61 ± 0.71	6.87 ± 1.10	7.11 ± 1.59	8.30 ± 1.29†	8.77 ± 0.67†‡*
Vw (mm)	23.35 ± 3.92	24.65 ± 3.24	26.32 ± 2.87	29.87 ± 3.60†	32.74 ± 4.11†‡*
VBd (mm)	6.03 ± 0.98	5.86 ± 0.81	5.67 ± 0.65	6.42 ± 0.68	6.66 ± 0.53
Vd (mm)	21.34 ± 2.72	20.61 ± 1.86	21.20 ± 2.41	22.78 ± 2.54	24.39 ± 2.27‡
SCw (mm)	10.27 ± 0.94	10.82 ± 0.83	11.11 ± 0.79	12.00 ± 1.04†	12.12 ± 1.61†
SCd (mm)	8.08 ± 0.86	7.99 ± 0.66	7.93 ± 0.90	8.12 ± 0.83	8.18 ± 0.96
VBh (mm)	7.35 ± 1.70	6.26 ± 1.25	6.18 ± 1.47	6.32 ± 1.76	6.07 ± 1.36
IVDh (mm)	2.31 ± 0.21	2.18 ± 0.12	2.23 ± 0.25	2.25 ± 0.15	2.21 ± 0.15
Vw/Vd	1.10 ± 0.19	1.19 ± 0.09	1.25 ± 0.10	1.31 ± 0.12	1.34 ± 0.11
VBd/Vd	0.29 ± 0.05	0.28 ± 0.04	0.27 ± 0.03	0.28 ± 0.03	0.27 ± 0.02
VBw/Vw	0.29 ± 0.05	0.28 ± 0.04	0.27 ± 0.02	0.28 ± 0.01	0.27 ± 0.03
VBw/VBd	1.12 ± 0.19	1.18 ± 0.17	1.26 ± 0.17	1.29 ± 0.11	1.32 ± 0.16
VBh/VBd	1.21 ± 0.15	1.06 ± 0.14	1.08 ± 0.19	0.97 ± 0.20	0.93 ± 0.19†
SCw/SCd	1.27 ± 0.07	1.36 ± 0.10	1.41 ± 0.12	1.48 ± 0.07†	1.49 ± 0.15†
SCw/Vw	0.45 ± 0.05	0.44 ± 0.04	0.43 ± 0.04	0.40 ± 0.03	0.37 ± 0.04†‡
SCd/Vd	0.38 ± 0.05	0.39 ± 0.03	0.38 ± 0.03	0.36 ± 0.03	0.34 ± 0.03‡
IVDh/VBh	0.33 ± 0.11	0.36 ± 0.08	0.38 ± 0.11	0.38 ± 0.10	0.38 ± 0.08

Mean ± SD. Significant differences among vertebral segments in monkey are shown as C3 (†), and C4 (‡), C5 (\*) ( $P < 0.05$ ). Shaded cells demonstrate a significant difference between the monkey and the human ( $P < 0.05$ ). A one-way ANOVA was used to compare the parameters among segments, and a post hoc Bonferroni test was used when there were significant differences on a one-way ANOVA. Kruskal-Wallis test was used to compare the ratios among segments, and a post hoc Dunn's test was used for multiple comparisons.

**Table 5.** Cervical anatomical measurements and ratios obtained by MRI in monkey

	C3	C4	C5	C6	C7
SCow (mm)	9.59 ± 0.50	9.79 ± 0.42	9.92 ± 0.44	9.84 ± 0.40	9.26 ± 0.92
SCod (mm)	6.32 ± 0.30	6.42 ± 0.40	6.32 ± 0.40	6.58 ± 0.44	6.57 ± 0.57
ACFd (mm)	1.09 ± 0.16	1.14 ± 0.19	1.16 ± 0.20	1.26 ± 0.19	1.20 ± 0.15
PCFd (mm)	1.16 ± 0.12	1.09 ± 0.14	1.08 ± 0.17	1.05 ± 0.13	1.30 ± 0.22*#
SCwM (mm)	12.13 ± 0.75	12.47 ± 0.59	13.06 ± 0.92	14.02 ± 1.36†‡	13.79 ± 0.97†‡
SCdM (mm)	8.28 ± 0.21	8.12 ± 0.34	8.09 ± 0.54	8.57 ± 0.52	8.43 ± 0.69
SCow/SCod	1.52 ± 0.09	1.53 ± 0.09	1.57 ± 0.10	1.50 ± 0.08	1.41 ± 0.08*
SCow/SCwM	0.79 ± 0.06	0.79 ± 0.04	0.76 ± 0.05	0.71 ± 0.06†‡	0.67 ± 0.08†‡
SCod/SCdM	0.76 ± 0.04	0.79 ± 0.04	0.78 ± 0.06	0.77 ± 0.04	0.78 ± 0.08
CFd/SCod	0.36 ± 0.03	0.35 ± 0.04	0.35 ± 0.03	0.35 ± 0.03	0.38 ± 0.05

Mean ± SD. Significant differences among vertebral segments in monkey are shown as C3 (†), and C4 (‡), C5 (\*), and C6 (#) ( $P < 0.05$ ). Shaded cells demonstrate a significant difference between the monkey and the human ( $P < 0.05$ ). A one-way ANOVA was used to compare the parameters among segments, and a post hoc Bonferroni test was used when there were significant differences on a one-way ANOVA. Kruskal-Wallis test was used to compare the ratios among segments, and a post hoc Dunn's test was used for multiple comparisons. Note: CFd = ACFd + PCFd.

macaques, might also contribute to this because a greater axial area can decrease bending stresses. This is further supported by the fact that the vertebral body occupied a larger portion of the vertebrae (VBw/Vw and VBd/Vd) in the human subjects compared with the macaques.

Spinal cord morphology is of great importance for establishing the type of spinal cord injury, especially bilateral or unilateral contusion and hemisection models [32–36]. More precise parameters are needed to generate, with high repeatability, a unilateral contusion model that enables further study of limb function and a higher survival rate [12, 37, 38]. Our results, specifically those for the SCw/SCd ratio, showed that the axial morphology of the spinal cord was flatter in the human subjects than in the macaques. In addition, the trend of the changes in

the SCow/SCwM ratio from C3–C7 were different between human subjects and macaques, while the change trend of the SCod/SCdM ratio from C3–C7 was similar between the two species. The SCow/SCwM and SCod/SCdM ratios of the macaques were significantly greater than that of those of the human subjects, indicating that the spatial shift of the spinal cord in the spinal canal of the human subjects was larger than that of the macaques. Generally, the more available space for the spinal cord, the less likely it is to be crushed and injured. Therefore, when using macaques to establish a cervical spinal cord contusion model, more attention should be paid to the laminectomy process to expose the spinal cord than the clinical laminectomy process. Furthermore, the laminectomy window size in macaque models must be consistent

and appropriate, because lateral movement of the spinal cord during spinal contusion, especially in the case of a unilateral contusion, is a factor affecting the degree of injury consistency [11, 12].

The CSF space, defined as the thickness of the anterior cerebrospinal fluid and posterior cerebrospinal fluid, is a valuable parameter for assessing the spinal cord to coordinate mechanical readings of a contusion device, locate the dural touch and the cord touch, and maintain cord stability [12]. Three cases of rhesus macaques (*Macaca mulatta*) with pre-operative MRIs were measured by Salegio *et al.* [12], and the average CSF space was evaluated to be 1.2 mm on the posterior side (PCFd) and 0.9 mm on the anterior side (ACFd) at the C5 level, respectively. In our study, examination of 10 macaques revealed that the thickness of the cerebrospinal fluid was  $1.16 \pm 0.20$  mm on the anterior side (ACFd) and  $1.08 \pm 0.17$  mm (PCFd) on the posterior side of the C5 region, respectively. In addition, we found that the proportion of cerebrospinal fluid in the human spinal cord (CFd/SCod) was significantly greater than that in the macaques (70% in the human subjects; 40% in the macaques). This information can be used to determine the contact force when establishing a contusion spinal cord injury model by controlling displacement [11, 12, 39]. This could be used to set the contact force such that the spinal cord is close to the bottom of the spinal canal during contusion, reducing the movement of the spinal cord and thereby reducing the impact of the cerebrospinal fluid on the degree of contusion; this would make the established model more consistent and accurate. In other words, the CSF space acts a pivotal part in generating models with moderately severe contusion injury in macaques.

Tominaga *et al.* [19] measured the anatomical dimensions of cadaveric cervical spines in human subjects and found that the average width and depth of the spinal canal from C3 to C7 were 3.03 mm and 2.50 mm larger than those measured in our study (width,  $23.19 \pm 2.77$  mm; depth,  $12.72 \pm 1.66$  mm). Differences in measurement methods and samples may contribute to the discrepancy. In addition, the previous study showed that the SCw/SCd ratio reflecting the morphology of the cervical spinal canal in human subjects, was 1.74 [19], whereas in our study, the values determined by CT and MRI were 1.85 and 1.72, respectively, indicating similarity in the spinal canal morphology between these studies.

There were some limitations in the present study. The subjects in this study were adult males, and other genders and age groups were not considered. In addition, the number of samples in this study might not have been sufficient. Increasing the number of samples could make the data more convincing. More importantly, in this

study, the macaques subjected to micro-CT were sourced from cadaveric specimens, and this was inconsistent with the human CT data sources. CT is more accurate for observing bone structure, while MRI is more accurate for observing soft tissue. In this study, the same parameters, such as the maximum width and depth of the spinal canal, were measured by CT and MRI, and the results showed different tendencies (CT and MRI:  $1.85 \pm 0.27$  and  $1.72 \pm 0.15$  for human subjects and  $1.40 \pm 0.13$  and  $1.58 \pm 0.15$  for macaques, respectively). A possible reason for this is that CT and MRI data were not from the same individuals; alternatively, it is possible that there was an inconsistency in the measurement accuracy between the two methods for the same structure.

The morphology of the vertebral body, spinal canal, and spinal cord parenchyma of the cervical spine in the macaques was different from that in the human subjects. However, the trends of the changes in the segments of the cervical spine were similar between the macaques and human subjects. Our study provides anatomical parameters of the cervical spine in macaques that may be helpful in designing future studies using the cervical spine of the macaque as an alternative model of the human cervical spine. In addition, when establishing pre-clinical research models of spinal cord injury in macaques, these parameters can also provide a basis for surgical operations and contusion parameter settings.

### Compliance with Ethical Standards

This research was approved by the Institutional Animal Care And Use Committee (IACUC) of Guangdong Landau Biotechnology Co., Ltd., and the Ethics Committee of Nanfang Hospital, Southern Medical University. The permission number was LD-ZA-2016-01.

### Conflicts of Interest

All authors declare no competing financial interests.

### Acknowledgments

This study was supported by the National Natural Science Foundation of China (No. 81972064).

### References

1. Alam M, Garcia-Alias G, Jin B, Keyes J, Zhong H, Roy RR, et al. Electrical neuromodulation of the cervical spinal cord facilitates forelimb skilled function recovery in spinal cord injured rats. *Exp Neurol.* 2017; 291: 141–150. [Medline] [CrossRef]
2. Gruber HE, Phillips R, Ingram JA, Norton HJ, Hanley EN Jr. Spontaneous age-related cervical disc degeneration in the

- sand rat. *Clin Orthop Relat Res.* 2014; 472: 1936–1942. [Medline] [CrossRef]
3. Kamiyama T, Kameda H, Murabe N, Fukuda S, Yoshioka N, Mizukami H, et al. Corticospinal tract development and spinal cord innervation differ between cervical and lumbar targets. *J Neurosci.* 2015; 35: 1181–1191. [Medline] [CrossRef]
  4. Showalter BL, Beckstein JC, Martin JT, Beattie EE, Espinoza Orias AA, Schaer TP, et al. Comparison of animal discs used in disc research to human lumbar disc: torsion mechanics and collagen content. *Spine.* 2012; 37: E900–E907. [Medline] [CrossRef]
  5. Bozkus H, Crawford NR, Chamberlain RH, Valenzuela TD, Espinoza A, Yüksel Z, et al. Comparative anatomy of the porcine and human thoracic spines with reference to thoracoscopic surgical techniques. *Surg Endosc.* 2005; 19: 1652–1665. [Medline] [CrossRef]
  6. Kumar N, Kukreti S, Ishaque M, Mulholland R. Anatomy of deer spine and its comparison to the human spine. *Anat Rec.* 2000; 260: 189–203. [Medline] [CrossRef]
  7. Talac R, Friedman JA, Moore MJ, Lu L, Jabbari E, Windbank AJ, et al. Animal models of spinal cord injury for evaluation of tissue engineering treatment strategies. *Biomaterials.* 2004; 25: 1505–1510. [Medline] [CrossRef]
  8. Dienstag JL, Davenport FM, McCollum RW, Hennessy AV, Klatskin G, Purcell RH. Nonhuman primate-associated viral hepatitis type A. Serologic evidence of hepatitis A virus infection. *JAMA.* 1976; 236: 462–464. [Medline] [CrossRef]
  9. Pauthner M, Havenar-Daughton C, Sok D, Nkolola JP, Bastidas R, Boopathy AV, et al. Elicitation of robust Tier 2 neutralizing antibody responses in nonhuman primates by HIV envelope trimer immunization using optimized approaches. *Immunity.* 2017; 46: 1073–1088.e6, e1076. [Medline] [CrossRef]
  10. Forný-Germano L, Lyra e Silva NM, Batista AF, Brito-Moreira J, Gralle M, Boehnke SE, et al. Alzheimer's disease-like pathology induced by amyloid- $\beta$  oligomers in nonhuman primates. *J Neurosci.* 2014; 34: 13629–13643. [Medline] [CrossRef]
  11. Liu J, Li R, Huang Z, Huang Z, Li Y, Wu X, et al. A Cervical Spinal Cord Hemi-Contusion Injury Model Based on Displacement Control in Non-Human Primates (*Macaca fascicularis*). *J Neurotrauma.* 2020; 37: 1669–1686. [Medline] [CrossRef]
  12. Salegio EA, Bresnahan JC, Sparrey CJ, Camisa W, Fischer J, Leasure J, et al. A unilateral cervical spinal cord contusion injury model in non-human primates (*Macaca mulatta*). *J Neurotrauma.* 2016; 33: 439–459. [Medline] [CrossRef]
  13. Kalin NH, Shelton SE. Nonhuman primate models to study anxiety, emotion regulation, and psychopathology. *Ann N Y Acad Sci.* 2003; 1008: 189–200. [Medline] [CrossRef]
  14. Goncharova ND, Marenin VY, Oganyan TE. Aging of the hypothalamic-pituitary-adrenal axis in nonhuman primates with depression-like and aggressive behavior. *Aging (Albany NY).* 2010; 2: 854–866. [Medline] [CrossRef]
  15. Cox LA, Olivier M, Spradling-Reeves K, Karere GM, Comuzzie AG, VandeBerg JL. Nonhuman Primates and Translational Research-Cardiovascular Disease. *ILAR J.* 2017; 58: 235–250. [Medline] [CrossRef]
  16. Hansen BC. Progressive nature of obesity and diabetes in nonhuman primates. *Obesity (Silver Spring).* 2017; 25: 663–664. [Medline] [CrossRef]
  17. Ding SY, Tigno XT, Hansen BC. Nuclear magnetic resonance-determined lipoprotein abnormalities in nonhuman primates with the metabolic syndrome and type 2 diabetes mellitus. *Metabolism.* 2007; 56: 838–846. [Medline] [CrossRef]
  18. Muthumani K, Falzarano D, Reuschel EL, Tingey C, Flingai S, Villarreal DO, et al. A synthetic consensus anti-spike protein DNA vaccine induces protective immunity against Middle East respiratory syndrome coronavirus in nonhuman primates. *Sci Transl Med.* 2015; 7: 301ra132. [Medline] [CrossRef]
  19. Tominaga T, Dickman CA, Sonntag VK, Coons S. Comparative anatomy of the baboon and the human cervical spine. *Spine.* 1995; 20: 131–137. [Medline] [CrossRef]
  20. Thomas CE, Combs CM. Spinal cord segments. B. Gross structure in the adult monkey. *Am J Anat.* 1965; 116: 205–216. [Medline] [CrossRef]
  21. Nalley TK, Grider-Potter N. Functional analyses of the primate upper cervical vertebral column. *J Hum Evol.* 2017; 107: 19–35. [Medline] [CrossRef]
  22. Nakatsukasa M, Hayama S, Preuschoft H. Postcranial skeleton of a macaque trained for bipedal standing and walking and implications for functional adaptation. *Folia Primatol (Basel).* 1995; 64: 1–29. [Medline] [CrossRef]
  23. Meyer MR, Woodward C, Tims A, Bastir M. Neck function in early hominins and suspensory primates: Insights from the uncinat process. *Am J Phys Anthropol.* 2018; 166: 613–637. [Medline] [CrossRef]
  24. Manfreda E, Mitteroecker P, Bookstein FL, Schaefer K. Functional morphology of the first cervical vertebra in humans and nonhuman primates. *Anat Rec B New Anat.* 2006; 289: 184–194. [Medline] [CrossRef]
  25. Beckstein JC, Sen S, Schaer TP, Vresilovic EJ, Elliott DM. Comparison of animal discs used in disc research to human lumbar disc: axial compression mechanics and glycosaminoglycan content. *Spine.* 2008; 33: E166–E173. [Medline] [CrossRef]
  26. Jaumard NV, Leung J, Gokhale AJ, Guarino BB, Welch WC, Winkelstein BA. Relevant anatomic and morphological measurements of the rat spine: considerations for rodent models of human spine trauma. *Spine.* 2015; 40: E1084–E1092. [Medline] [CrossRef]
  27. Sheng SR, Xu HZ, Wang YL, Zhu QA, Mao FM, Lin Y, et al. Comparison of cervical spine anatomy in calves, pigs and humans. *PLoS One.* 2016; 11: e0148610. [Medline] [CrossRef]
  28. Flynn JR, Bolton PS. Measurement of the vertebral canal dimensions of the neck of the rat with a comparison to the human. *Anat Rec (Hoboken).* 2007; 290: 893–899. [Medline] [CrossRef]
  29. Graf W, de Waele C, Vidal PP, Wang DH, Evinger C. The orientation of the cervical vertebral column in unrestrained awake animals. II. Movement strategies. *Brain Behav Evol.* 1995; 45: 209–231. [Medline] [CrossRef]
  30. Ferrario VF, Sforza C, Serrao G, Grassi G, Mossi E. Active range of motion of the head and cervical spine: a three-dimensional investigation in healthy young adults. *J Orthop Res.* 2002; 20: 122–129. [Medline] [CrossRef]
  31. Stemper BD, Yoganandan N, Pintar FA, Maiman DJ, Meyer MA, DeRosia J, et al. Anatomical gender differences in cervical vertebrae of size-matched volunteers. *Spine.* 2008; 33: E44–E49. [Medline] [CrossRef]
  32. Borbély Z, Csomó BK, Kittel Á, Gerber G, Varga G, Vizi ES. Effect of rat spinal cord injury (hemisection) on the ex vivo uptake and release of [ $^3$ H]noradrenaline from a slice preparation. *Brain Res Bull.* 2017; 131: 150–155. [Medline] [CrossRef]
  33. Liu H, Schwarz EM, Xie C. Dual differentiation-exogenous mesenchymal stem cell therapy for traumatic spinal cord injury repair in a murine hemisection model. *Stem Cells Int.* 2013; 2013: 928982. [Medline] [CrossRef]
  34. Moon HC, Lee YJ, Cho CB, Park YS. Suppressed GABAergic signaling in the zona incerta causes neuropathic pain in a thoracic hemisection spinal cord injury rat model. *Neurosci Lett.* 2016; 632: 55–61. [Medline] [CrossRef]
  35. Teh DBL, Chua SM, Prasad A, Kakkos I, Jiang W, Yue M, et al. Neuroprotective assessment of prolonged local hypothermia post contusive spinal cord injury in rodent model. *Spine J.* 2018; 18: 507–514. [Medline] [CrossRef]
  36. Zareen N, Shinozaki M, Ryan D, Alexander H, Amer A, Truong DQ, et al. Motor cortex and spinal cord neuromodulation promote corticospinal tract axonal outgrowth and motor re-

- covery after cervical contusion spinal cord injury. *Exp Neurol.* 2017; 297: 179–189. [[Medline](#)] [[CrossRef](#)]
37. Detloff MR, Quiros-Molina D, Javia AS, Daggubati L, Nehlsen AD, Naqvi A, et al. Delayed exercise is ineffective at reversing aberrant nociceptive afferent plasticity or neuropathic pain after spinal cord injury in rats. *Neurorehabil Neural Repair.* 2016; 30: 685–700. [[Medline](#)] [[CrossRef](#)]
38. Watson JL, Hala TJ, Putatunda R, Sannie D, Lepore AC. Persistent at-level thermal hyperalgesia and tactile allodynia accompany chronic neuronal and astrocyte activation in superficial dorsal horn following mouse cervical contusion spinal cord injury. *PLoS One.* 2014; 9: e109099. [[Medline](#)] [[CrossRef](#)]
39. Huang Z, Li R, Liu J, Huang Z, Hu Y, Wu X, et al. Longitudinal electrophysiological changes after cervical hemi-contusion spinal cord injury in rats. *Neurosci Lett.* 2018; 664: 116–122. [[Medline](#)] [[CrossRef](#)]